THEORETICAL AND MATERIAL STUDIES ON THIN-FILM ELECTROLUMINESCENT DEVICES

Second Six Monthly Report for the Period
1 October 1985 - 31 March 1986

Project No. A-4168

Prepared for:

Dr. J. B. Robertson/494
NASA
Langley Research Center
Hampton, VA 23665

Prepared by:

Dr. C. J. Summers* and Dr. K. F. Brennan+
Georgia Institute of Technology
Atlanta, GA 30332

July 1986

*Georgia Tech Research Institute and Microelectronics Research Center

+School of Electrical Engineering and Microelectronics Research Center

(NASA-CR-177150) THEORETICAL AND MATERIAL STUDIES ON THIN-FILM ELECTROLUMINESCENT DEVICES Biannual Report, 1 Oct. 1985 - 31 Mar. 1986 (Georgia Inst. of Tech.) 37 p CSCL 09A G3/33

N86-30932

Unclas 43499

CONTENTS

1. INTRODUCTION

This report for the period 1 October 1985 through 31 March 1986 reports on the work performed during the second six-months of NASA Contract NAG-1-586, under the technical direction of Dr. J. B. Robertson.

The principal co-investigators of this study were Drs. C. J. Summers and K. F. Brennan, who were assisted in part by several graduate students, Mr. H. D. Rodgers, Mr. B. K. Wagner and Mr. R. G. Benz.

The report briefly describes the theoretical and experimental progress made so far.

2. THEORETICAL MODELING STUDIES OF VARIABLY SPACED SUPERLATTICE STRUCTURES

This study consumed most of our effort during this report period and was emphasized because it was essential to obtain an accurate model of the VSSEF structure in order to fully explore the viability of this concept. The work proved to be more involved than anticipated and, because of its complexity, was initially applied to the AlGaAs system so that comparisons could be made with some previous, but less complete studies. The results of this study produced the submission of a paper to the Journal of Applied Physics and also the acceptance of a paper to be presented at the Second International Meeting on Superlattices, Microstructures and Devices, in Goteburg, Norway during August.

Copies of the paper and abstract complete this section.

THEORY OF RESONANT TUNNELING IN A VSSEF MULTIQUANTUM WELL STRUCTURE: AN AIRY FUNCTION APPROACH

K. F. Brennan[1]
and
C. J. Summers[2]

Microelectronics Research Center
Georgia Institute of Technology
Atlanta, Georgia 30332

ABSTRACT

A theoretical study of resonant tunneling in multilayered heterostructures is presented based on an exact solution of the Schroedinger equation under the application of a constant electric field. By use of the transfer matrix approach, the transmissivity of the structure is determined as a function of the incident electron energy. The approach presented herein is easily extended to many layer structures where it is more accurate than other existing transfer matrix or WKB models. The transmission resonances are compared to the bound state energies calculated for a finite square well under bias using either an asymmetric square well model or the exact solution of an infinite square well under the application of an electric field. The results show good agreement with other existing models as well as with the bound state energies. The calculations were then applied to a new superlattice structure, the variably spaced superlattice energy filter, VSSEF, which is designed such that under bias the spatial quantization levels fully align. Based on these calculations, a new class of resonant tunneling superlattice devices can be designed.

---

1 School of Electrical Engineering.

2 Georgia Tech Research Institute.

I. INTRODUCTION

Since the advent of exacting epitaxial growth techniques, particularly MBE and MOCVD, realization of superlattice and multiquantum well structures has become possible. The superlattice, as originally proposed by Esaki and Tsu [1], has found wide application in many new device structures such as photodetectors [2-5], transistors [6,7], and light emitters [8]. The most thoroughly studied material system as applied to superlattices is the GaAs/$Al_xGa_{1-x}As$ system owing to the relative ease in its fabrication as well as its close lattice matching. Under the application of a bias, carriers can tunnel through these structures provided that the wider gap AlGaAs layers are sufficiently thin. However, to optimize the current flow in a multiwell structure, the adjacent energy levels within the GaAs wells, arising from spatial quantization effects must be aligned. Several experimental measurements have recently confirmed the presence of resonant tunneling in single and double quantum well structures [9-12]. Optical absorption measurements [13] have also independently verified the formation of superlattice minibands arising from the coupling of adjacent quantum states.

The theories used to explain resonant tunneling phenomena generally break down into three different approaches, use of the WKB approximation [14,15], which is valid if the barrier energy varies slowly compared to the scale of the electron wavelength, a Monte Carlo solution of the semiclassical Boltzmann transport equation [16,17], in which a quasi-particle picture of the electron is assumed, and the transfer matrix approach which gives the transmissivity of the structure as a function of energy directly. The WKB approximation is not valid in the device structures of greatest interest, those with narrow barriers. The Monte Carlo approach is useful since it

includes phonon scattering but does not easily lend itself to the calculation of the structure's transparency.

Tsu and Esaki [18] first provided a theoretical description of the electron tunneling current density in a multilayer structure. Their approach involves the solution of the Schroedinger equation in each region of the device under the assumptions that the applied bias is small (allowing for the use of plane wave and evanescent wave solutions), the effective mass is constant throughout, and phonon scattering can be neglected. The tunneling transmission coefficient is then determined by the transfer matrix method; a 2 x 2 matrix at each interface is formed by matching the continuity of the wavefunctions and their derivatives. Successive multiplication of these matrices then couples the incident wavevector to the outgoing wavevector of the heterostructure stack. The current density is calculated from the transmission coefficient τ for a one-dimensional system as [18],

$$J = \frac{em^* kT}{2\pi^2\hbar^3} \int_0^\infty \tau \ \ln\left(\frac{1 + \exp(E_f - E_1)/kT}{1 + \exp(E_f - E_1 - eV_a)/kT}\right) dE_1 \qquad (1)$$

where E_F is the Fermi energy, E_1 the energy of the N = 1 subband, V_a the overall applied bias, T the temperature, and m^* the effective mass of the carrier.

Mukherji and Nag [19] reformulated the calculations retaining a staircase potential shape (plane wave and evanescent wave solutions are used throughout) but added the effect of band nonparabolicities and differing masses within the layers. Their method is mathematically similar to that of Esaki and Tsu [18] in that a transfer matrix approach is used. Vassel et al. [20] have further extended the transfer matrix model by computing the transmission coefficient

from direct numerical calculation of the 2 x 2 transfer matrices. Thus, their approach is directly applicable to arbitrary potential profiles. However, good numerical convergence near the turning points is difficult to achieve and may lead to significant error in many layered stacks [21].

The exact solution of a particle in a uniform static field is well known and can be expressed as a linear combination of Airy and complementary Airy functions [18]. The solution of the infinite square well under an applied field is then expressible in terms of Airy functions. There are two independent means of determining the energies in a quantum well, a direct Airy function solution which becomes exact for an infinite square well [22,23], and a transmission resonance calculation. Miller et al. [23] have found excellent agreement between the two models provided that effective widths are chosen for the infinite square well such that the correct finite square well zero field energies result.

Recently a new superlattice structure has been proposed, the variably spaced superlattice energy filter (VSSEF) [24]. In this structure, the energy levels arising from spatial quantization effects become resonantly aligned under bias. By varying the narrow gap layer widths, and hence the energies of the quantum levels, the quantum states in adjacent wells are designed to be separated in energy by the voltage drop across each cell, thus resulting in their alignment under the appropriate bias voltage. This structure has the advantage of providing a high speed resonant tunneling channel under bias as opposed to the original Esaki-Tsu constant period superlattice [18] which is resonantly aligned only at zero or very low bias. As shown by Döhler et al. [25] in a constant period superlattice, if the voltage drop across each period is greater than the miniband width, the transport changes from Bloch-like

propagation to "hopping" conduction. It is expected that "hopping" conduction is slower than resonant tunneling. Therefore, a VSSEF structure should provide better performance than a constant period superlattice under large bias.

We present resonant tunneling transmissivity calculations in a VSSEF-like superlattice structure made from the GaAs/AlGaAs material system. The calculations are based on an exact Airy function solution to the Schroedinger equation using the transfer matrix approach. The calculations are described in detail in Section II. As a control on our calculations in Section III, the Airy function solution is compared to that of Vassel et al. [20] and also to the predicted energy levels using an uncoupled finite square well calculation. In Section IV, the transmissivity of a six and eight period VSSEF superlattice is calculated. The results clearly show the resonant tunneling transition. As the bias varies from the critical voltage, under which the levels align, the transmissivity peaks broaden away from the sharp resonant levels. Finally, the conclusions are presented in Section V.

II. MODEL DESCRIPTION

The calculation is performed in a straightforward way by solving the Schroedinger equation exactly in each region (barrier and well) and then matching the continuity of the wavefunction and its derivative at each boundary. A representative multilayer stack is diagrammatically presented in Figure 1. The solution of the Schroedinger equation in region one is simply a linear combination of an incident and reflected plane wave,

$$\psi_1 = e^{ik_1 x} + Re^{-ik_1 x} \tag{2}$$

where $k_1 = \sqrt{2m_1E/\hbar^2}$ and m_1 is the effective mass in the narrow gap (GaAs) layer. The Schroedinger equation in region two can be written as,

$$\psi_2''(\rho) - \rho\psi_2(\rho) = 0 \tag{3}$$

where

$$\rho = \left(\frac{2m_2eV_a}{L\hbar^2}\right)^{1/3}(x + \eta) \; ; \; \eta = (L/eV_a)(V_o - E_\ell)$$

eV_a/L is the applied electric field, V_o is the barrier height, and x is the real space distance measured from the interface between regions 1 and 2. The solution is readily expressed in terms of Airy functions as,

$$\psi_2(\rho) = C_2^+Ai(\rho) + C_2^-Bi(\rho) \tag{4}$$

Within region 3, the Schroedinger equation becomes,

$$\psi_3''(\rho) + \rho\psi_3(\rho) = 0 \tag{5}$$

where

$$\rho = \left(\frac{2m_1eV_a}{L\hbar^2}\right)^{1/3}(x + \eta) \; ; \; \eta = (E_\ell + b^*eV_a/L)/(eV_a/L)$$

and b is the barrier width. In this case, x is now measured with respect to the second interface. The solution in this region is then,

$$\psi_3(\rho) = C_3^+Ai(-\rho) + C_3^-Bi(-\rho) \tag{6}$$

The solution in all succeeding regions is the same then as either that in region 2 or in region 3.

The imposition of the boundary conditions at $x = 0$ (the interface between region 1 and region 2) gives,

$$1 + R = C_2^+ Ai_2(x = 0) + C_2^- Bi_2(x = 0)$$

$$ik(1 - R) = C_2^+ Ai_2'(x = 0) + C_2^- Bi_2'(x = 0) \tag{7}$$

which in matrix form becomes,

$$\begin{pmatrix} 1 \\ R \end{pmatrix} = \frac{-1}{2ik} \begin{pmatrix} -ik & -1 \\ -ik & 1 \end{pmatrix} \begin{pmatrix} Ai_2(x=0) & Bi_2(x=0) \\ Ai_2'(x=0) & Bi_2'(x=0) \end{pmatrix} \begin{pmatrix} C_2^+ \\ C_2^- \end{pmatrix} \tag{8}$$

Extending the analysis to a multiple well system gives,

$$\begin{pmatrix} 1 \\ R \end{pmatrix} = \frac{1}{2ik} \begin{pmatrix} ik & 1 \\ ik & -1 \end{pmatrix} S_2(x = 0) S_2^{-1}(x = b) S_3(x = 0) S_3^{-1}(x = a_1)$$

$$S_2(x = 0) S_2^{-1}(x = b) S_3(x = 0) S_3^{-1}(x = a_2) \cdots S_2(x = 0) S_2^{-1}(x = b) \tag{9}$$

$$\begin{pmatrix} 1 & 1 \\ ik' & -ik' \end{pmatrix} \begin{pmatrix} \tau \\ 0 \end{pmatrix}$$

where the matrices S_2 and S_3 are defined as,

$$S_2(x) = \begin{bmatrix} Ai(\rho) & Bi(\rho) \\ Ai'(\rho) & Bi'(\rho) \end{bmatrix} \tag{10}$$

(ρ is given as in equation (3));

$$S_3(x) = \begin{bmatrix} Ai(-\rho) & Bi(-\rho) \\ Ai'(-\rho) & Bi'(-\rho) \end{bmatrix}$$

(ρ is given as in equation (5)).

The subsequent product of the transfer matrices (S_2 and S_3) is found. The resulting expression becomes,

$$\begin{pmatrix} 1 \\ R \end{pmatrix} = \frac{1}{2ik} \begin{pmatrix} ik & 1 \\ ik & -1 \end{pmatrix} S(0,L) \begin{pmatrix} 1 & 1 \\ ik' & -ik' \end{pmatrix} \begin{pmatrix} \tau \\ 0 \end{pmatrix} \tag{11}$$

using the notation of Vassel et al. [20] for the product of the S matrices. Note that equation (11) is essentially the inverse to equation (12) in Vessel et al. [20]. From equation (11) the transmissivity, τ, can be found noticing that $\tau = k/k'1./M_{11}^2$ where the matrix M is

$$M = \frac{1}{2ik} \begin{pmatrix} ik & 1 \\ ik & -1 \end{pmatrix} S(0,L) \begin{pmatrix} 1 & 1 \\ ik' & -ik' \end{pmatrix} \tag{12}$$

Therefore, τ is given by,

$$\tau = \frac{4k/k'}{(A + k'/kD)^2 + (C/k - k'B)^2}$$

where A, B, C, D are the elements of the S(0,L) matrix. Finally, the tunneling current density can be obtained through substitution in equation (1).

III. MODEL COMPARISON

It is useful to compare the resonant tunneling calculation, as outlined in Section II, to the calculation of Vassel et al. [20] and to the calculated

bound state energies in a finite square well under the application of an applied electric field. Resonances in the transmissivity vs. electron energy curve correspond to the bound state energies in the wells. Additionally, the width of these resonances determines the broadening of the energy levels. The transmission resonances in one and multiwell structures are presented below and are compared to Vassel's model [20] and to two different bound state energy calculations.

The logarithm of the transmission coefficient as a function of energy in a one well, two barrier $GaAs/Al_xGa_{1-x}As$ structure is presented in Figure 2. The structure analyzed is identical to that used by Vassel et al. [20]. The calculation is performed under two conditions, the masses are assumed equal to the GaAs mass in the wells and barriers, $m_1 = m_2 = 0.067\ m_o$, and different masses in the layers are considered, $m_1 = 0.067\ m_o$, $m_2 = 0.1087\ m_o$. It is expected that the different mass model more nearly approximates the physical situation since the energy wavevector dispersion relation is different between the barrier and the well. The use of an effective mass remains valid even for energies in the forbidden band as is the case in the barrier region [20]. Figure 2 shows that at an applied bias of 0.16 V two resonances appear in the transmissivity. The peaks appear systematically at higher energy than that calculated by Vassel et al. [20]. The resonances are also shifted upwards in energy in the two mass model from those calculated using the one mass model. This can be easily understood as follows. A larger mass value within the barrier region (the case for the GaAs/AlGaAs material system) is equivalent mathematically to choosing a greater potential barrier height and subsequently a deeper potential well energy. As is well known, the bound state energies within the infinite square well lie at higher energy than the corresponding

finite square well states. Thus, as the well depth increases, the bound state energy levels increase in energy.

The calculation is repeated at a higher bias, 0.4 V, in Figure 3. Again, the resonance energy is shifted to higher energy in the Airy function approach as compared to that of Vassel et al. [20]. In this case, only one peak in the transmission coefficient occurs. As the bias increases, the resonances appear at lower energy owing to the conduction band bending under the action of the electric field. For 0.4 V bias, the N = 1 level lies below the Fermi level and is, therefore, no longer in alignment with E_F, thus the first resonance completely disappears as can be seen in Figure 4. The results again confirm that the resonance peak occurs at higher energy in the two mass model.

From Figures 2 and 3, it is apparent that the Airy function approach agrees reasonably well with the approach of Vassel et al. [20] in predicting the location of the transmission resonances. It is necessary, however, to check the agreement with the bound state energies in a finite square well under the application of an electric field. Being that an exact solution of the bound state energy in a finite square well under bias is not possible, three different approaches can be used to estimate the energy. A straightforward application of time independent perturbation theory proves useless in determining the energy at sizeable electric field strengths. Numerous terms in the perturbation expansion are required which is impractical. Alternatively, a finite square well under bias can be treated as an asymmetric square well; the potential barrier is higher on one side of the well than on the other side. This problem can be solved analytically [20,22] for the well width in terms of the energy level and barrier heights as [22],

$$ka = n\pi - \sin^{-1}\left(\hbar k/\sqrt{2mU_1}\right) - \sin^{-1}\left(\hbar k/\sqrt{2mU_2}\right) \qquad (13)$$

U_1 and U_2 are the potential barrier heights, a is the well width, and k is the $\vec{k}$ vector corresponding to the energy level. The bound state energies in an asymmetric square well of equivalent dimensions to those calculated using the resonant tunneling approach are shown in Figure 4. At 0.16 V bias, the n = 1 state is shifted (after subtracting the band bending) to 0.00855 eV while the n = 2 state is shifted to 0.289 eV. Both calculations are well below the corresponding tunneling resonance values. However, Kelly [26] has shown that an asymmetric square well deviates significantly from an exact Airy function calculation. Therefore, it is expected that the asymmetric square well approach is not a wholly reliable means of determining the bound state energies within the system.

Miller et al. [23] have adopted an alternative approach using the exact solution of the infinite square well under bias. In principle, the eigenstates of an infinite quantum well under bias are exactly determinable, however, the solution is generally quite difficult to obtain. Excellent agreement is obtained with the tunneling calculation if the infinite square well width is adjusted such that the bound state energies correspond to those in a finite square well [23]. The bound state energies are obtained using a variational calculation [27]. From this calculation, a universal result for the binding energy as a function of the normalized field induced energy is obtained [27]. The location of the n = 1 quantum states in our single well system under the application of a constant bias are readily determined from Figure 1 in Reference 27. After subtracting off the band bending due to the bias (the energy level is measured with respect to the band minimum), the

n = 1 levels occur at 0.03 eV at 0.16 V bias, and at -0.108 eV at 0.40 V bias (Figure 4). This result agrees more favorably with our resonant tunneling calculation.

The transmission coefficient as a function of energy for a two well, three barrier system at 0.16 and 0.4 V bias is presented in Figure 5. Similar qualitative agreement is obtained with the results of Vassel et al. [20]. Again, it is interesting to note that the resonances occur at higher energy in the Airy function calculation than in the numerical approach of Vassel et al. [20]. It has been shown by Kelly [26] that the Airy function approach shows much finer detail than either the WKB method or the stepped (asymmetric) quantum well method. In addition, since the calculation is exact, no convergence errors at the turning points are introduced, thus making this calculation more suited to multiple well structures.

IV. VSSEF CALCULATIONS

A representative diagram of the VSSEF structure is presented in Figure 6. As can be seen from the figure, the energy level scheme is designed (by varying the well widths) such that under bias all of the n = 1 levels align. As mentioned above, this provides a resonant tunneling channel through the superlattice structure. It is expected that for a VSSEF device, designed to show alignment of the n = 1 levels, that only at certain bias will the transmissivity be sharp. As the bias is either increased or decreased from this value then the structure becomes dealigned leading to a broader transmissivity.

In a superlattice, miniband formation arises from the coupling of the energy levels in adjacent quantum wells. From a plot of the transmission

coefficient versus the incident electron energy, the transmission resonances can be determined. Figures 7-9 show the transmission coefficient for a six well, seven barrier GaAs/$Al_{0.45}Ga_{0.55}As$ superlattice. The barrier height is chosen to be 0.347 eV in accordance with the 60/40 rule [28]. The effective masses are 0.067 and 0.1067 in the GaAs and AlGaAs layers, respectively. The device dimensions are chosen by designing the structure such that adjacent levels align. The wells are first assumed to be uncoupled. Equation (13) can then be used to determine the well widths necessary for alignment to occur at a fixed bias, in this case, 0.20 volts. These dimensions are used in the resonant tunneling calculation in which full coupling is considered to obtain the structure's transmissivity. The calculated results using equation (13) are not exact since use of it assumes that the wells are uncoupled. However, it provides an estimate as to a structure which will align under bias.

The tunneling calculation shows that as the bias changes from 0.16 V to 0.20 V (Figures 7-9), the low energy (n = 1) transmissivity peak changes dramatically. At 0.16 V, roughly four separate peaks arise (Figure 7). As the bias increases to 0.18 V, only two sharp peaks closely spaced in energy appear (Figure 8). Further increase in bias results in the reappearance of four peaks broadening the transmission resonance once again. These figures clearly show that the structure resonantly aligns at a fixed bias. As the voltage changes away from this value (0.18 V in this case), the structure becomes resonantly dealigned reflected by the broadening of the transmissivity peaks.

The calculation is repeated for an eight well, nine barrier structure. The tunneling transmission resonances are plotted versus incident electron energy in Figures 10-14 at different biases, 0.16-0.20 V. Again, a resonant

tunneling transition can be observed at 0.17 V. At 0.17 V bias, the four peaks occur evenly spaced in energy and have approximately the same magnitude (excepting one). As the number of wells increases, the number of states common to the superlattice increases as well. It is expected that sharp coincidence of these states is progressively more difficult to achieve under bias. The calculations presented herein indicate that sharper alignment is achieved in the six well case as opposed to the eight well case.

Sharp alignment of the transmissivity peaks, as demonstrated by Tsu and Esaki [18] for a constant period superlattice at zero bias, cannot be attained as neatly in a VSSEF structure. This is due to two limitations. First, it is not definite that the devices presented above have perfect alignment of each quantum level since the method used to design the well widths (equation (13)) is not precise. Most likely, the levels are reasonably aligned but perhaps not fully. This will result in some splitting in the transmissivity peaks. Additionally, since the quantum wells have different widths, it is not clear that the wavefunctions corresponding to each quantum well contribute equally to the net superlattice wavefunction. This explains the lack of as sharply defined resonance peaks in the VSSEF calculations as compared to that within a constant period superlattice [18].

IV. CONCLUSIONS

A solution to the resonant tunneling problem is presented based on the exact solution of the Schroedinger equation within the potential wells and barriers of a multilayered heterojunction stack. Good qualitative agreement is obtained with previous models. In addition, the calculated resonances agree fairly well with the calculated bound state energies derived from the

solution of the infinite square well under bias. The Airy function approach shows much finer structure than either the WKB or potential step models of previous workers. The Airy function approach is apparently better suited to many layered structures (since it has no convergence error) as well as narrow barrier structures in which the WKB approximation becomes invalid.

The first theoretical verification of the resonant alignment of the variably spaced superlattice energy filter, VSSEF, has been presented. The VSSEF structure becomes resonantly aligned under bias as opposed to the traditional constant period superlattice which is resonantly aligned only at zero or low applied bias. The transport within the VSSEF device is Bloch-like. Hence, the VSSEF is much faster than a "hopping" transport superlattice, a constant period superlattice biased such that the voltage drop within each period exceeds the miniband width. Based upon these calculations, new high speed resonant tunneling devices can be designed. Future work will address the design of electroluminescent devices, avalanche photodiodes, and IMPATT structures based on the VSSEF concept and the calculations presented herein.

ACKNOWLEDGEMENTS

The authors are greatly indebted to Dr. M. O. Vassel for many helpful discussions. The authors would like to thank H. D. Rogers for his assistance in the solution of the Schroedinger equation using Airy functions. In addition, the authors would like to thank B. K. Wagner for computational help. The technical assistance of Peggy Knight at the Georgia Institute of Technology is gratefully acknowledged. This work was sponsored in part by NASA under contract NAG-1-586.

FIGURE CAPTIONS

Figure 1: Schematic representation of a multilayer stack for purposes of discussion concerning the tunneling current calculations.

Figure 2: Logarithm of the transmission coefficient as a function of incident electron energy for a one well structure at an applied bias of 0.16 V. The curve shows the location of the transmission resonances in both the Airy function model and the model of Vassel et al. [20].

Figure 3: Logarithm of the transmission coefficient as a function of incident electron energy for a one well structure at an applied bias of 0.4 V. The curve shows the location of the transmission resonances in both the Airy function model, as well as the model of Vassel et al. [20].

Figure 4: Diagram showing the calculated bound state energies in a finite square well under a) zero bias, b) 0.16 V bias, and c) 0.40 V bias.

Figure 5: Logarithm of the transmission coefficient as a function of incident electron energy at 0.16 V and 0.40 V bias to a two well, three barrier device. Again, the Airy function model and that of Vassel et al. [20] are compared.

Figure 6: Schematic representation of the VSSEF structure. a) Device geometry; b) zero bias; c) applied bias, $eV \sim E_I$.

Figures 7-9: Logarithm of the transmission coefficient as a function of incident electron energy at 0.16 V, 0.18 V, and 0.20 V bias for a six well, seven barrier VSSEF structure. The well widths are 139 Å, 45.7 Å, 35.3 Å, 29.1 Å, 24.8 Å, and 21.4 Å.

The barrier widths are all 20 Å wide. Notice that the transmissivity sharpens to two closely spaced peaks at low energy at 0.20 V bias. This is the signature of the resonant alignment of the device.

Figures 10-14: Logarithm of the transmission coefficient as a function of incident electron energy at 0.16 V, 0.17 V, 0.18 V, 0.19 V, and 0.20 V bias for an eight well, nine barrier VSSEF structure. The well widths are 148.3 Å, 52.5 Å, 41.0 Å, 34.2 Å, 29.5 Å, 26.0 Å, 23.0 Å, and 20.7 Å, At 0.17 V bias, the peaks at low energy approach one another in magnitude thus signifying the resonance condition.

REFERENCES

1. L. Esaki and R. Tsu, IBM J. Res. Dev., 14, 61 (1970).
2. R. Chin, N. Holoyak, Jr., G. E. Stillman, J. Y. Tang, and K. Hess, Electron. Lett., 16, 467 (1980).
3. F. Capasso, W. T. Tsang, A. L. Hutchinson, and G. F. Williams, Appl. Phys. Lett., 40, 38 (1982).
4. F. Capasso, K. Mohammed, A. Y. Cho, R. Hull, and A. L. Hutchinson, Appl. Phys. Lett., 47, 420 (1985).
5. J. S. Smith, L. C. Chiu, S. Margalit, and A. Yariv, J. Vac. Sci. Technol. B1, 376 (1983).
6. F. Capasso and R. A. Kiehl, J. Appl. Phys., 58, 1366 (1985).
7. M. Heiblum, D. C. Thomas, C. M. Knoedler, and M. I. Nathan, Appl. Phys. Lett., 47, 1105 (1985).
8. K. Ploog and G. H. Döhler, Advances in Physics, 32, 285 (1983).
9. T. C. L. G. Sollner, W. D. Goodhue, P. E. Tannenwald, C. D. Parker, and D. D. Peck, Appl. Phys. Lett., 43, 588 (1983).
10. L. L. Chang, L. Esaki, and R. Tsu, Appl. Phys. Lett., 24, 593 (1974).
11. E. A. Rezek, N. Holonyak, Jr., B. A. Vojak, and H. Shichijo, Appl. Phys. Lett., 31, 703 (1977).
12. B. A. Vojak, N. Holonyak, Jr., R. Chin, E. A. Rezek, R. D. Dupuis, and P. D. Dapkus, J. Appl. Phys. 50, 5835 (1979).
13. R. Dingle, A. C. Gossard, and W. Wiegmann, Phys. Rev. Lett., 34, 1327 (1975).
14. G. C. Osbourn, J. Vac. Sci. Technol., 17, 1104 (1980).
15. J. Heremans, D. L. Partin, and P. D. Dresselhaus, Appl. Phys. Lett., 48, 644 (1986).

16. P. J. Price, IBM J. Res. Develop., 17, 39 (1973).

17. M. Artaki and K. Hess, Superlattice and Microstructures, 1, 489 (1985).

18. R. Tsu and L. Esaki, Appl. Phys. Lett., 22, 562 (1973).

19. D. Mukherji and B. R. Nag, Solid-State Electronics, 21, 555 (1978).

20. M. O. Vassel, J. Lee, and H. F. Lockwood, J. Appl. Phys., 54, 5206 (1983).

21. M. O. Vassel, private communication.

22. L. O. Landau and E. M. Lifshitz, Quantum Mechanics - Nonrelativitistic Theory, (Pergamon, New York, 1981), Chapter VII.

23. D. A. C. B. Miller, D. S. Chemla, T. C. Damen, A. C. Gossard, W. Wiegmann, T. H. Wood, and C. A. Burrs, Phys. Rev. B, 32, 1043 (1985).

24. C. J. Summers and K. F. Brennan, Appl. Phys. Lett., 48, 806 (1986).

25. G. H. Döhler, R. Tsu, and L. Esaki, Solid State Commun., 17, 317 (1975).

26. M. J. Kelly, Electronics Letters, 20 (1984).

27. G. Bastard, E. E. Mendez, L. L. Chang, and L. Esaki, Phys. Rev. B, 28, 3241 (1983).

28. R. C. Miller, D. A. Kleinman, and A. C. Gossard, Phys. Rev. B, 29, 3740 (1984).

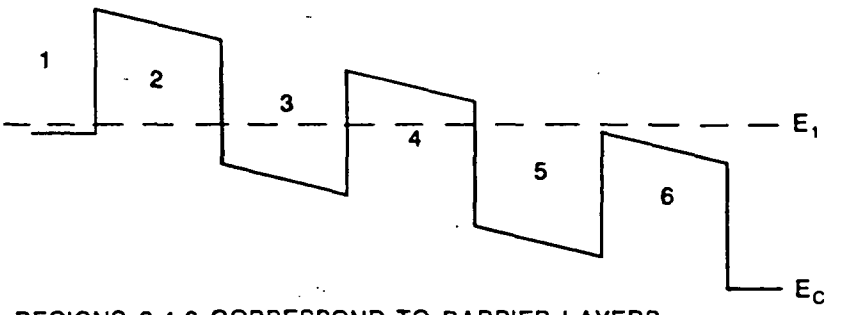

REGIONS 2,4,6 CORRESPOND TO BARRIER LAYERS.
1,3,5 CORRESPOND TO WELL LAYERS.

Brennan / Summers
Fig. 1

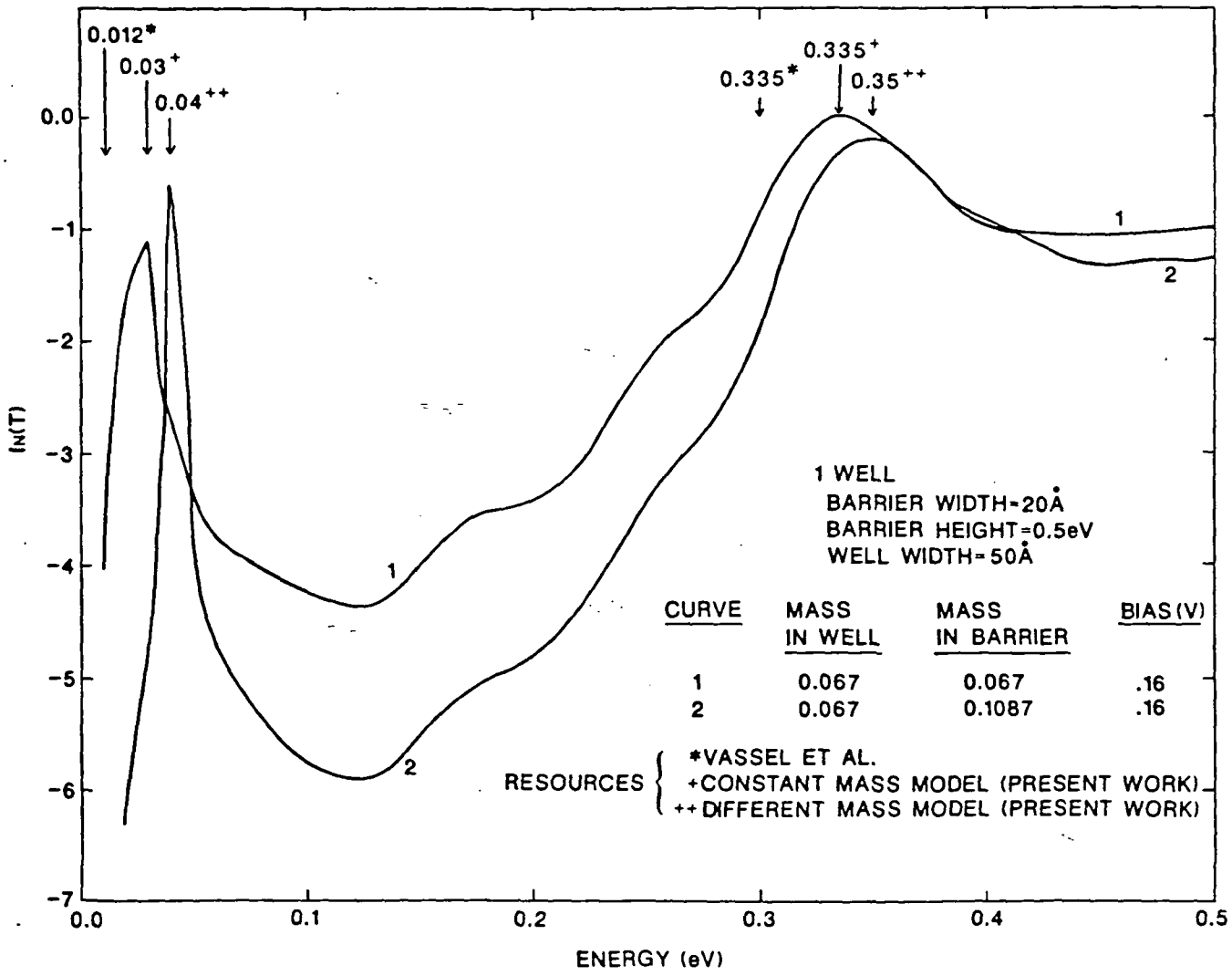

Brennan & Summers
Fig. 2

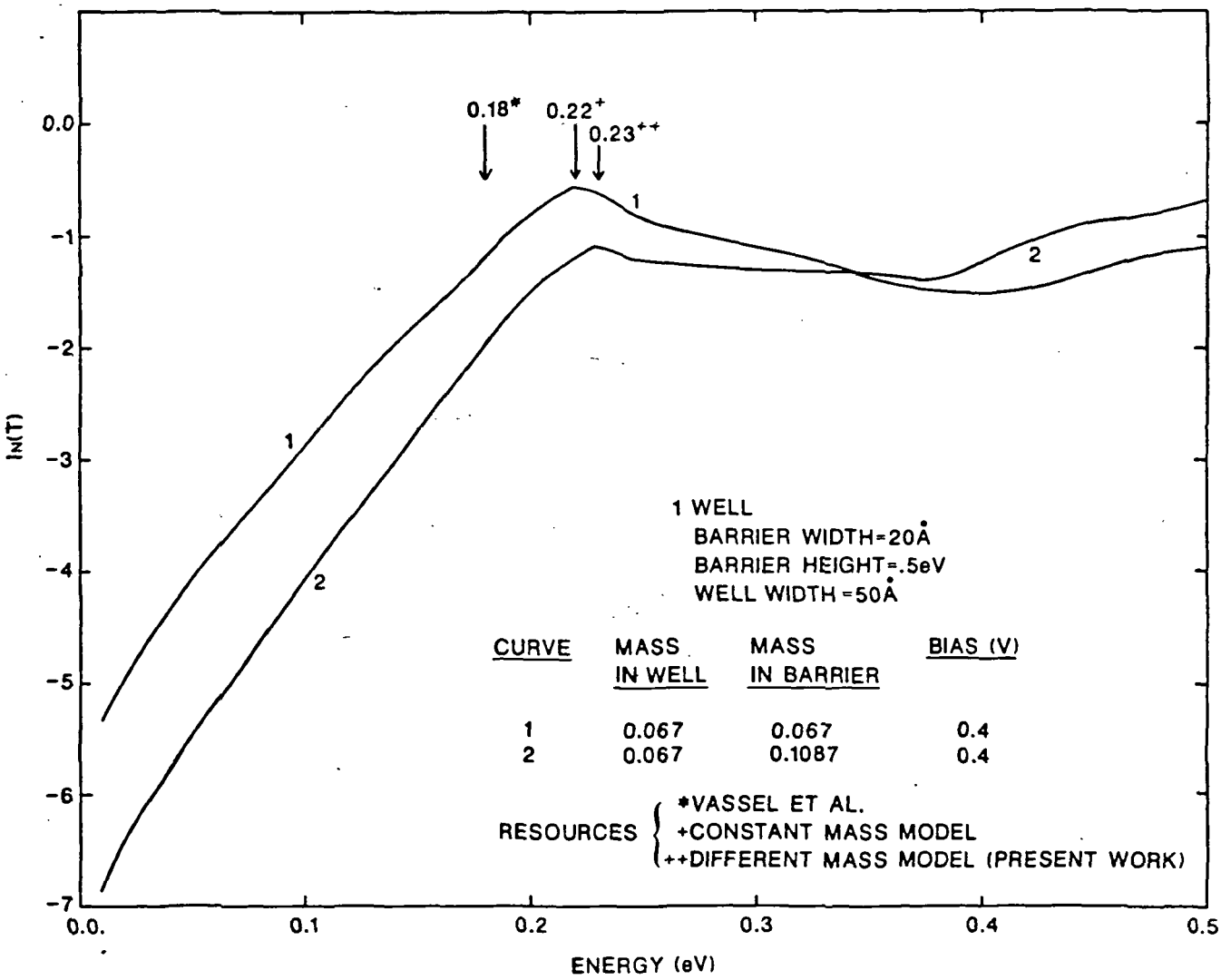

Brennan & Summers
Fig. 3

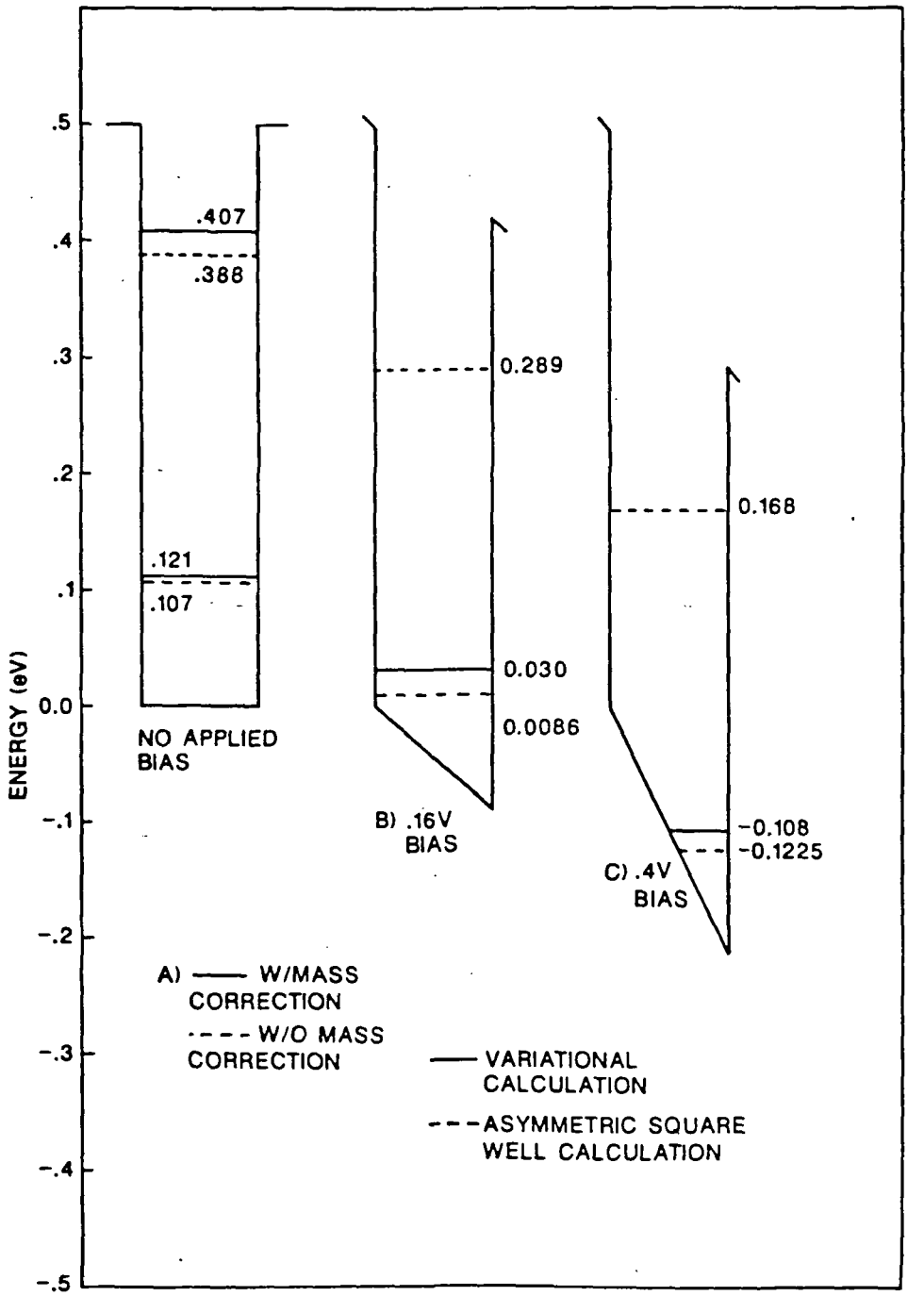

Brennan & Summers
Fig. 4

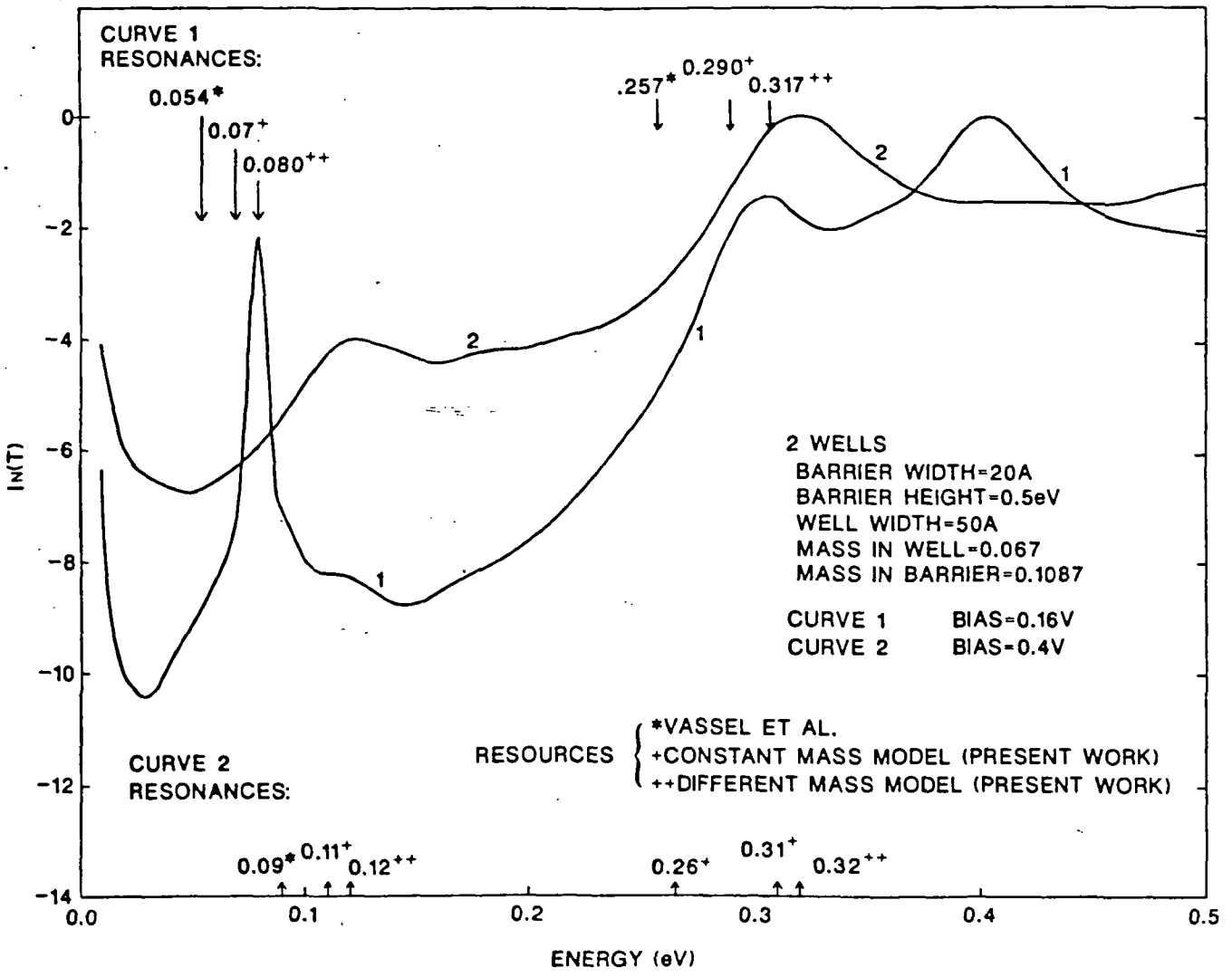

Brennan !
Summers
Fig. 5

(a)

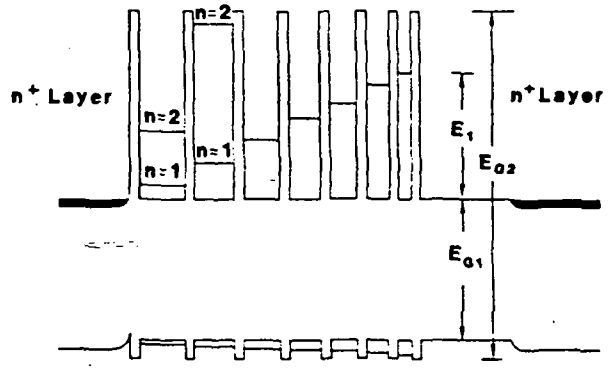

(b)

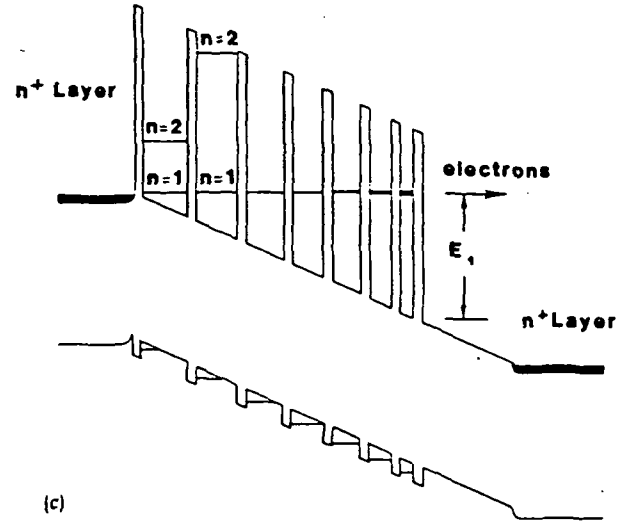

(c)

Brennan & Summers
Fig. 6

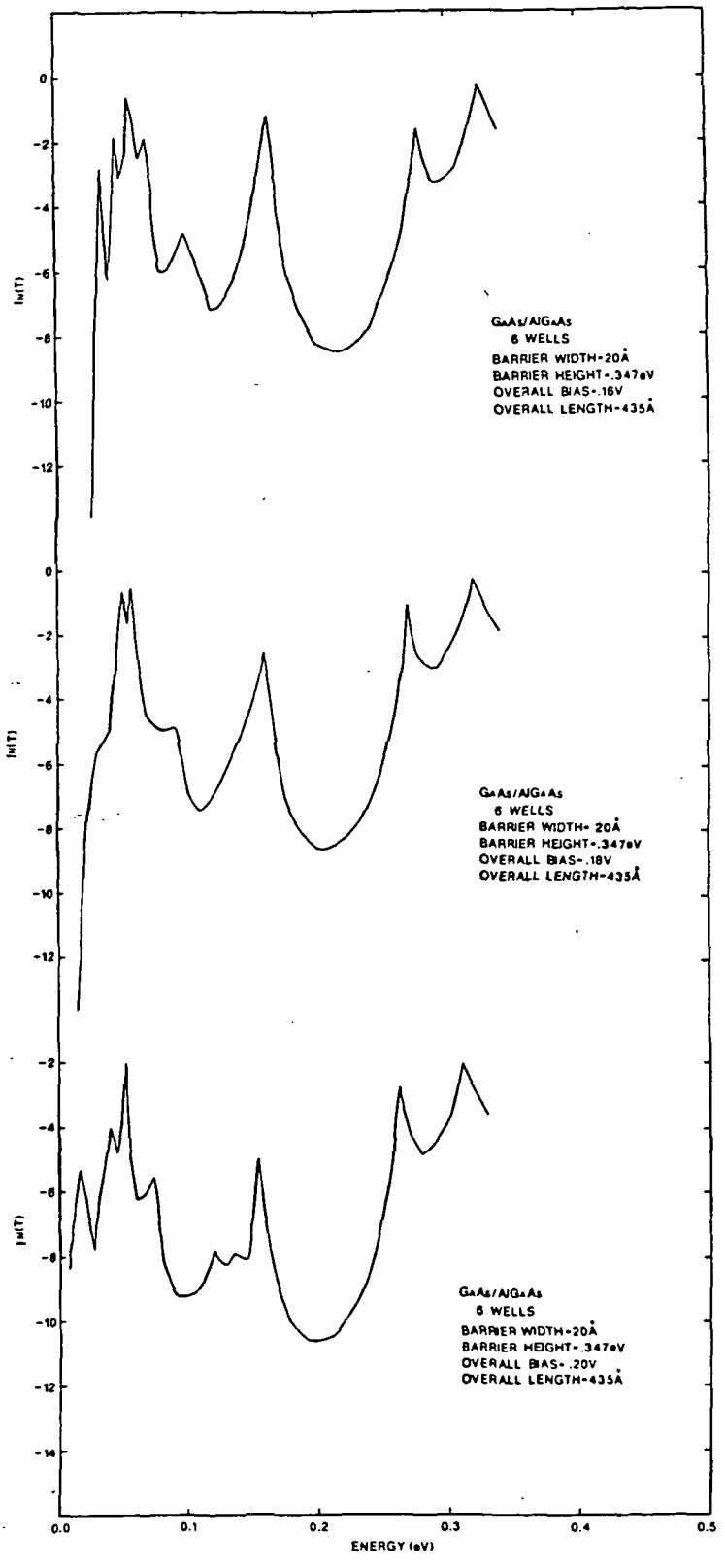

Brennan & Summers
Fig. 7-9

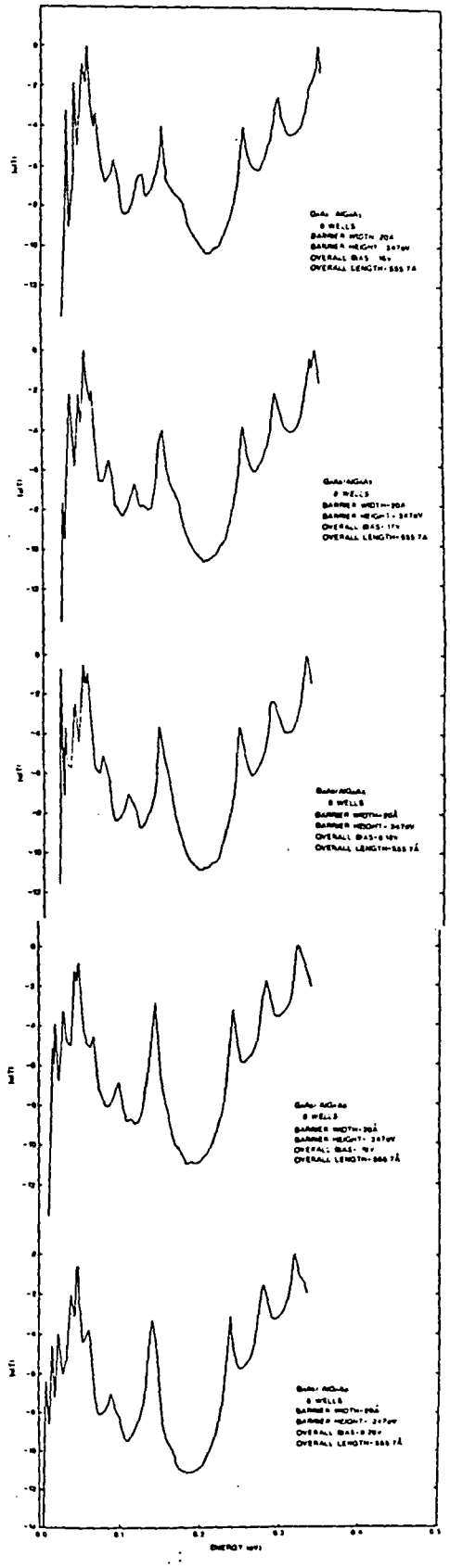

Barrier Summary Figs IC-14

3. GROWTH STUDIES

During this period, the MBE system previously used for CdTe growth studies was prepared for the growth of ZnS, ZnSe and also CaF_2 and SrF_2. Unfortunately, considerable difficulty was experienced in obtaining reproducible high-vacuum conditions in this system. These problems were traced to malfunctions in the main ion-pump and also the cryopumps used to pump the sample preparation chambers. Both of these items have been replaced and the system now has a stable base pressure of $<1x10^{-9}$ Torr. Also during this retrofit, a graphite furnace was added for evaporating flourides and improvements were made in the furnace temperature control system and flux monitor. Preliminary growth runs of ZnS on (001) GaAs substrates are in progress and will be reported in detail in the next report. A description of the system which is designed to perform studies of the surface growth conditions as well as to grow high quality epitaxial layers is shown in Figure 3.1 and described below.

As shown, the system consists of three interconnected vacuum chambers, a growth chamber, isolation chamber and introductionary chamber. The growth chamber is based on a Varian surface analytical chamber which has been extended to incorporate MBE growth furnaces and a sample load-lock mechanism. The advantage of this chamber is that there are four 4-inch diameter and four 1 1/2-inch diameter ports in the surface plane of the sample which gives good access to the substrate.

The growth chamber has a base pressure of $<10^{-10}$ Torr and has six ovens. The ovens, and the growth area, are surrounded by liquid nitrogen cooled shields to minimize cross-contamination and immediately condense excess vapors in the chamber. The desired growth fluxes are obtained by heating the furnaces and measuring the beam pressure from each oven with an ionization gauge which can be positioned at the sample growth position. A 10 KeV reflection high energy electron diffraction gun and screen are used to measure in-situ, the crystallographic properties of the substrate and growing MBE layer. The chemical composition,

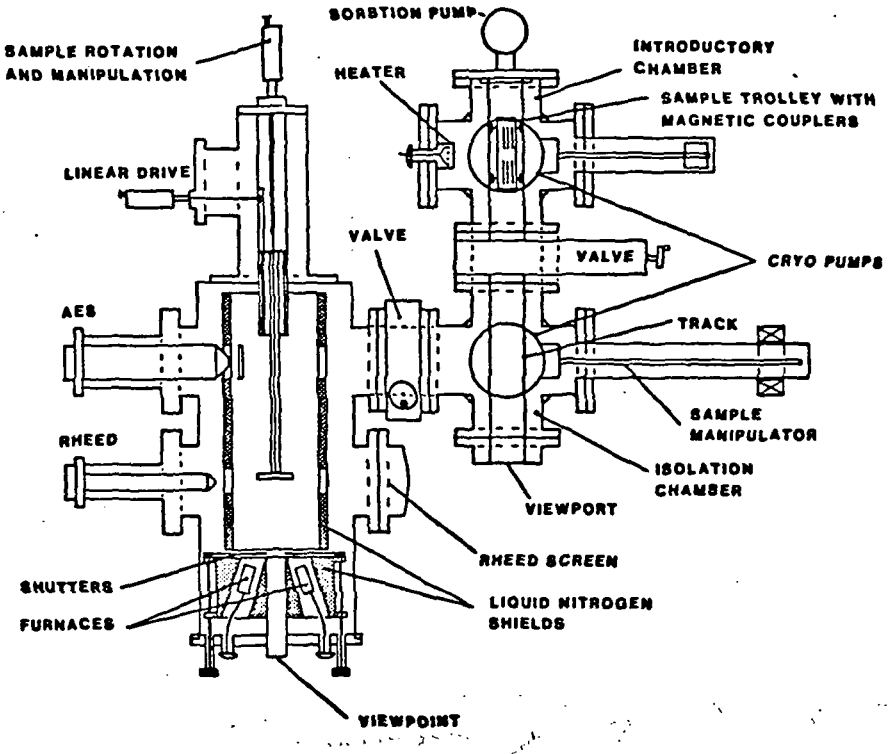

Figure 3.1. Schematic of the Analysis/MBE chamber used for surface studies of CdTe.

or contamination, of the substrate can be measured by the Auger spectrometer placed opposite the sample entry port. These measurements are possible without changing the temperature of the substrate but required that the sample be withdrawn approximately 7" down the main chamber and rotated 90^{o} to be at the focus of the analyzer.

The system is also equipped with a retractable ion-gauge for absolute flux measurement when placed in the growth position and a residual gas analyzer (RGA) to identify and measure the concentration of impurities remaining in the chamber.

From the above description it is apparent that to accomplish all of the required sample treatments and analyses it is necessary to manipulate the sample into several positions. To perform these manipulations, the substrate holder is mounted on a trolley which runs on a track down the center of the chamber. The position of the trolley is controlled by a rack and pinion drive placed on the side of the chamber. Two rotatory vacuum feed-throughs placed at the end of the chamber drive, through collapsable rods, a gear mechanisms at the sample head which enables 90^{o} left or right turns in a vertical plane, and also continuous sample rotation when facing the MBE furnaces. These controls give the motions needed to mount or dismount samples, or to take AES measurements. The sample rotation is required to align certain crystallographic directions in the surface plane of the substrate with the electron beam in order to obtain meaningful analysis of the RHEED data; this rotation can also be used to rotate the sample during growth.

To obtain optimum use of the apparatus and maintain reproducible ultra high vacuum conditions (i.e., low contamination levels) in the analysis/growth chamber, the sample is introduced through a two stage load-lock. This is shown on the right hand side of Figure 3.1. At present, this load-lock arrangement allows five samples to be loaded at a time but can be expanded to accommodate more samples. The samples are mounted vertically on a trolley which runs along the center of the introductory and isolation chambers.

The introductory chamber is rapidly evacuable to $<10^{-7}$ Torr by use of a cryopump and contains a heater for preliminary substrate and substrate holder degassing. By using the magnetic manipulator, a substrate can be removed from the trolley, placed on the heater, degassed, and then replaced back onto the trolley. After all the samples have been degassed, the introductionary chamber is pumped to its lowest pressure and the trolley is transferred into the isolation chamber by a magnetic transfer mechanism. Thus, the samples are stored in the isolation chamber, which is kept in the 10^{-9} Torr range by a cryopump. A substrate is introduced or removed from the analysis/growth chamber by using the magnetic coupler positioned opposite the main gate valve.

4. FUTURE WORK

In the next six months of the program a strong emphasis will be placed on the growth and characterization of ZnS films by MBE as well as the continuation of the modeling studies. Specific tasks to be performed are listed below.

1. Attempt to design a realistic TFEL-device structure using the theory recently formulated for resonant tunneling in quantum well structures in an electric field.

2. Grow (001) ZnS on (001) GaAs substrates for substrate temperatures between 300-500^{o}C at growth rates of 0.5-2 um/hr. Evaluate material properties by X-ray rocking curves, SEM, photoluminescence and cathodoluminescence.

3. Repeat 2, for Mn doping up to concentrations of 2-5%.

4. Investigate the use of (001) Si substrates.

5. Perform preliminary growth studies of CaF_2 and SrF_2.